Hindawi
International Journal of Chemical Engineering
Volume 2018, Article ID 6213568, 8 pages
https://doi.org/10.1155/2018/6213568

Research Article

Synthesis of Wollastonite Powders by Combustion Method: Role of Amount of Fuel

Imarally V. de S. R. Nascimento,[1,2] **Willams T. Barbosa**,[1,2] **Raúl G. Carrodeguas**,[1] **Marcus V. L. Fook**,[1] **and Miguel A. Rodríguez**[2]

[1]*CERTBIO, Universidade Federal de Campina Grande, Campina Grande, Brazil*
[2]*Instituto de Cerámica y Vidrio (CSIC), Madrid, Spain*

Correspondence should be addressed to Imarally V. de S. R. Nascimento; imarally.souza@hotmail.com

Received 29 March 2018; Accepted 24 July 2018; Published 9 September 2018

Academic Editor: Donald L. Feke

The objective of this work has been the synthesis of wollastonite by solution combustion method. The novelty of this work has been obtaining the crystalline phase without the need of thermal treatments after the synthesis. For this purpose, urea was used as fuel. Calcium nitrate was selected as a source of calcium and colloidal silica served as a source of silicon. The effect of the amount of fuel on the combustion process was investigated. Temperature of the combustion reaction was followed by digital pyrometry. The obtained products were characterized by scanning electron microscopy (SEM), X-ray diffraction (XRD), and specific surface area. The results showed that the combustion synthesis provides nanostructured powders characterized by a high surface area. When excess of urea was used, wollastonite-2M was obtained with a submicronic structure.

1. Introduction

The materials which are used to replace or supplement the functions of living tissues are known as biomaterials. To meet the requirement of an ideal biomaterial, it must be biocompatible, biodegradable, and bioactive, among others. One of the areas where biomaterials are used is in bone substitute or regeneration, which most often uses scaffolds. In this case, in addition to the intrinsic properties of the biomaterials, these must be osteoconductors and osteoinducers. Also, they must present an interconnected network of open porosity that is essential for cell nutrition, proliferation, and migration for tissue vascularization and providing mechanical support until formation of new tissues [1].

A variety of materials such as metals [2], ceramics [3], natural and synthetic polymers [4], and their combinations [5] have been explored for replacement and repair of damaged bone tissues. An extensive attention has been paid on the development of bioactive materials, including calcium phosphates, silicates, glasses, etc. which were used in the tissue regeneration applications [5, 6]. More attention has been paid on the calcium silicate ceramic materials, particularly wollastonite ($CaSiO_3$), used as a biomaterial for bone regeneration because of its excellent *in vitro* bioactivity. A lot of authors have studied their ability to induce formation of the hydroxyapatite layer on their surface *in vitro* conditions when immersed in simulated body fluid (SBF) with ion concentrations, pH, and temperature almost equal to those of human blood plasma [7–13].

It was demonstrated by De Aza and Luklinska [14], De Aza, Guitian, and De Aza [15, 16], and Wu et al. [17] that materials which contain Ca and Si atoms in their composition and which are free of P atoms can also produce HA layer on their surface. Fiocco et al. [9] proposes that the Mg atoms can further enhance the bioactivity of calcium-silicate materials.

Generally, calcium silicates are synthesized at high temperatures, between 900 and 1100°C. Wollastonite can be synthesized by the solid state route [18], sol gel [19], or coprecipitation method [20] but these methods require high energy and a long time for the formation of products.

Solution combustion synthesis (SCS) is widely used to synthesize submicronic oxide ceramic powders. This synthesis consists in an exothermic redox reaction, associated with the decomposition of nitrates (oxidants) and the oxidation of the fuel. The heat evolved is larger than that needed to maintain the combustion process; thus, the system becomes self-sustained. The chemical energy released from the exothermic reaction provides spontaneous synthesis [20–22]. The SCS has become an excellent technique for synthesis because of their inherent superior qualities, which include the better homogeneity, composition control, lower processing temperature, and single step operation, which result in high reactive powders [20, 23–25]. The final product is usually a crystalline material with nanometric size clusters and has a large specific surface area as a consequence of the large amount of gases produced during the synthesis process. This high volume of gases produces high porous agglomerates. The ignition temperature (T_{ig}) is significantly lower than the combustion temperature (T_c) which results in the final solid phase formation [23].

Chakradhar et al. [26] prepared macroporous nanocrystalline wollastonite ($CaSiO_3$) ceramic powders by a simple, low-temperature initiated, self-propagating, and solution combustion process. The phases of β-$CaSiO_3$ and α-$CaSiO_3$ were obtained only after heating at 950°C and 1200°C, respectively. Huang and Chang [22] synthesized wollastonite (α-$CaSiO_3$) by a citrate-nitrate gel combustion method using citric acid as a fuel and nitrate as an oxidant. The formation of α-$CaSiO_3$ was observed only after calcining powders at 650°C for 2 h.

The objective of this work was obtaining β-$CaSiO_3$ by combustion synthesis without the need of using further heating treatment. For this, $Ca(NO_3)_2$ and colloidal SiO_2 were employed as precursors and urea was used as fuel. The effect of the amount of fuel on the combustion process and characteristics of the products were studied as well.

2. Materials and Methods

Calcium nitrate tetrahydrate ($Ca(NO_3)_2.4H_2O$) (Neon Co., A.R. grade, 97%), colloidal SiO_2 (Sigma-Aldrich, Co., 50 wt% in water), urea (NH_2CONH_2) (Sigma-Aldrich, Co., A.R. grade, 99.5%), and nitric acid (HNO_3) (Sigma Aldrich, Co., A.R. grade 70%) were used as raw materials. The amounts of the reagents required to obtain 5 g of product were dissolved in 50 mL of deionized water.

The solution was dried and homogenized by stirring at 80°C to remove excess water. The beaker containing the solution was introduced into a muffle furnace preheated to 600°C. When placed in the furnace, the mixed solution soon started to boil, underwent dehydration, and the mass swelled to yield foam. The entire process required less than 15 min with flame duration of nearly one minute. The as-synthesized products were typically voluminous, fluffy foam-like mass that occupied a large volume. The resulting soft agglomerate was readily ground manually in an agate mortar/pestle into fine powder and was characterized.

2.1. Characterization. The phase composition of the prepared powders was determined by X-ray diffraction (XRD; Bruker D8) using nickel-filtered CuK_α radiation. Intensities were collected by step-scanning from 10° to 60° (2θ) with a step size of 0.02° and counting time of 1 s for each step. Fourier-transform infrared spectroscopy was obtained using a SPECTRUM 400 FTIR spectrometer. The samples were prepared at potassium bromide (KBr) pellets (ca. 2% by mass in KBr). The infrared spectra of prepared samples between 400 and 4000 cm^{-1} were recorded. The specific surface area (S_{BET}) of the powders was determined by nitrogen absorption (ASAP 2020M Analyzer, Micromeritics). The equivalent diameter (d_{BET}) of particle was calculated from the measured surface area (S_{BET}) values by using the following relationship:

$$d_{BET} = \frac{6}{S_{BET}\,\rho}, \tag{1}$$

where ρ is the theoretical density of the powder (2.8 g/cm^3 for the wollastonite). Field emission scanning electron microscopy (FESEM S-4700, Hitachi, Japan) was used to characterize the microstructure and morphology of the combustion product, which beforehand was coated with gold, by sputtering. Temperature profiles of the powder mixture were measured by a two-color pyrometer (IMPAC model IGAR 12-LO) that can measure temperature in the range 500°C–2200°C. The pyrometer was placed near the open door of the reactor furnace. The optics (with a glass fiber guide) was focused on the sample. Maximum flame temperatures were theoretically calculated for the combustion reactions with urea as fuel and for different ratios of fuel/oxidant. This was calculated from enthalpy of combustion reaction (ΔH°) and the heat capacity of products (C_p) at constant pressure.

3. Results and Discussion

The synthesis of wollastonite by combustion reaction can be represented by the (2):

$$\begin{aligned} &Ca(NO_3)_{2(aq)} + SiO_{2(s)} + \frac{5n}{2}(NH_2)_2CO_{(aq)} \\ &\quad + ((3n-2))HNO_{3(aq)} \longrightarrow CaSiO_{3(s)} + 4nN_{2(g)} \\ &\quad + \frac{5n}{2}CO_{2(g)} + \frac{13n-2}{2}H_2O_{(g)} \end{aligned} \tag{2}$$

where n is a coefficient that defines the total amount of fuel. This is related to the total released energy during the synthesis. The values of the coefficient n were 1, 2, and 3 for samples: $n = 1$ implies that the amount of urea required is the stoichiometric ratio of fuel to oxidant, considering aluminium nitrate as the only oxidant. $n = 2$ or 3 implies that the amount of fuel is twice and thrice, respectively, the stoichiometric one; in this case of fuel excess, corresponding amount of HNO_3 was added to balance the rest of fuel.

Available thermodynamic data in literature [27] of various reactants and products are listed in Table 1. Under adiabatic condition, the flame temperature (T_f) of

Table 1: Thermodynamic data employed in calculations [27].

Compound	ΔH_f (kJ/mol)	C_p (J/mol.K)
$Ca(NO_3)_2.4H_2O$	−2132.33	149.4
SiO_2	−903.49	43.975
$(NH_2)_2CO$	−333.51	92.79
HNO_3	−174.1	—
$CaSiO_3$	−1628.4	86.448
CO_2	−393.51	37.1
H_2O	−241.82	35.59
N_2	0	29.124

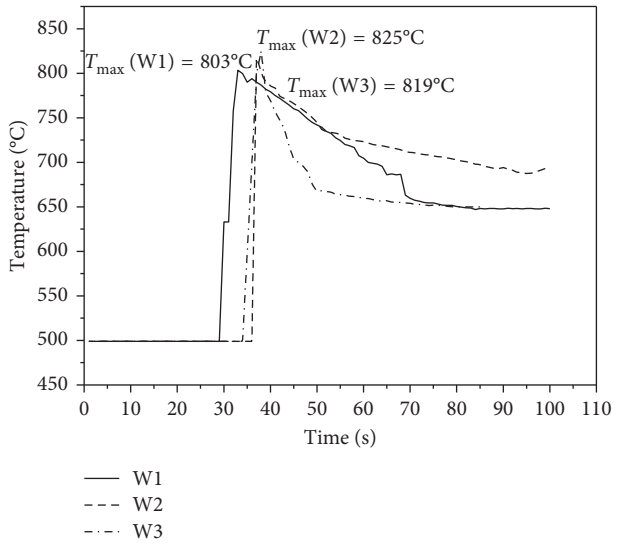

Figure 1: Time-temperature profile of aqueous solution combustion synthesis of wollastonite (initial furnace temperature of 600°C).

combustion systems for different contents of fuel was calculated by Equation (3):

$$Q = -\Delta H_{298} = \int_{T_0}^{T_{ad}} \left(\sum nC_p\right) dT, \quad (3)$$

where ΔH is given by $[\sum n\Delta H_f^o]_{products} - [\sum n\Delta H_f^o]_{reactants}$, ΔH_{298}° is the standard enthalpy of formation, C_p is the heat capacity of reaction products at constant pressure, and T_{ad} is the adiabatic flame temperature, in Kelvin scale (K).

The typical temperature-time profile for the solution combustion synthesis of $CaSiO_3$ is shown in Figure 1. Initially, it is observed that a short constant temperature region is the referred region where the temperature of the sample is lower than the minimum temperature range of the pyrometer. During this time, water is partially evaporated. Later, a sudden increase in temperature takes place up to a maximum value (T_{max}), and the synthesis is terminated with slow cooling.

The measured (T_c) and calculated flame temperatures (T_f) of this reaction and those with different fuel to oxidizer ratios are shown in Table 2. In all the profiles, it is observed that in the initial instants, the temperature verified by the pyrometer is of 500°C, although the furnace was at 600°C, and this difference of temperature is related to the fact that, initially, the sample was in a temperature lower than the minimum temperature measured by the pyrometer, which is 500°C. This period is also characterized by the evaporation of still remaining free water in the sample. When the material has not yet reached the furnace temperature, combustion begins. This increases rapidly from temperatures below 500°C to the maximum of combustion.

Table 2: Influence of n ratio on the maximum combustion temperature.

n ratio	Measured temperature (T_c) (°C)	Calculated temperature (T_f) (°C)
1	803	1664
2	819	2220
3	825	2453

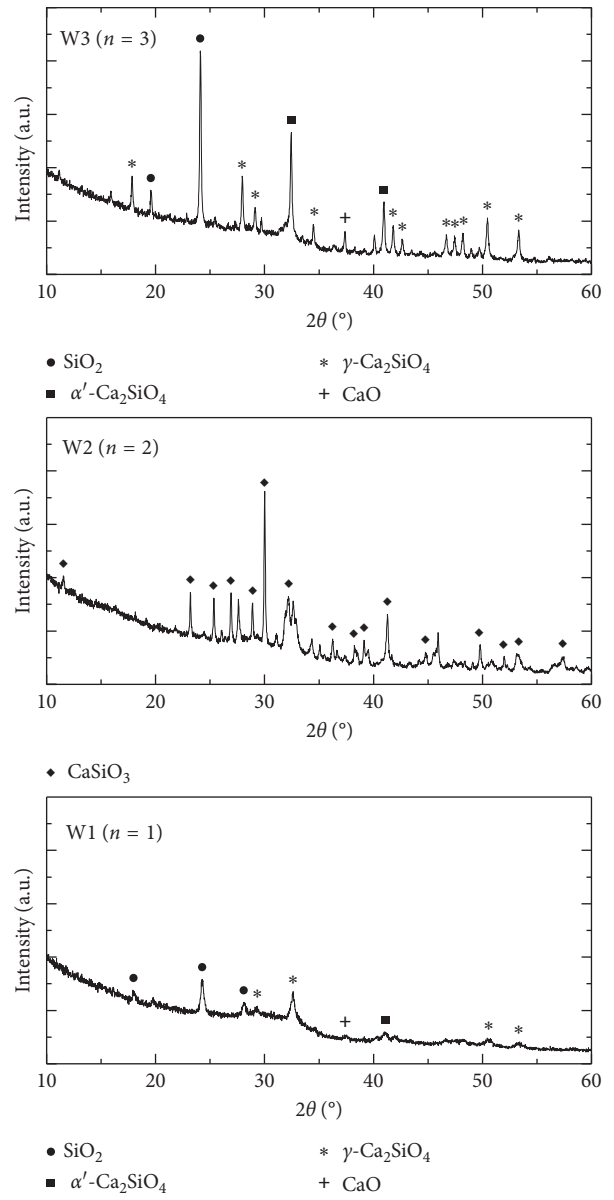

Figure 2: XRD patterns of combustion synthesis powders obtained from systems containing different amounts of urea.

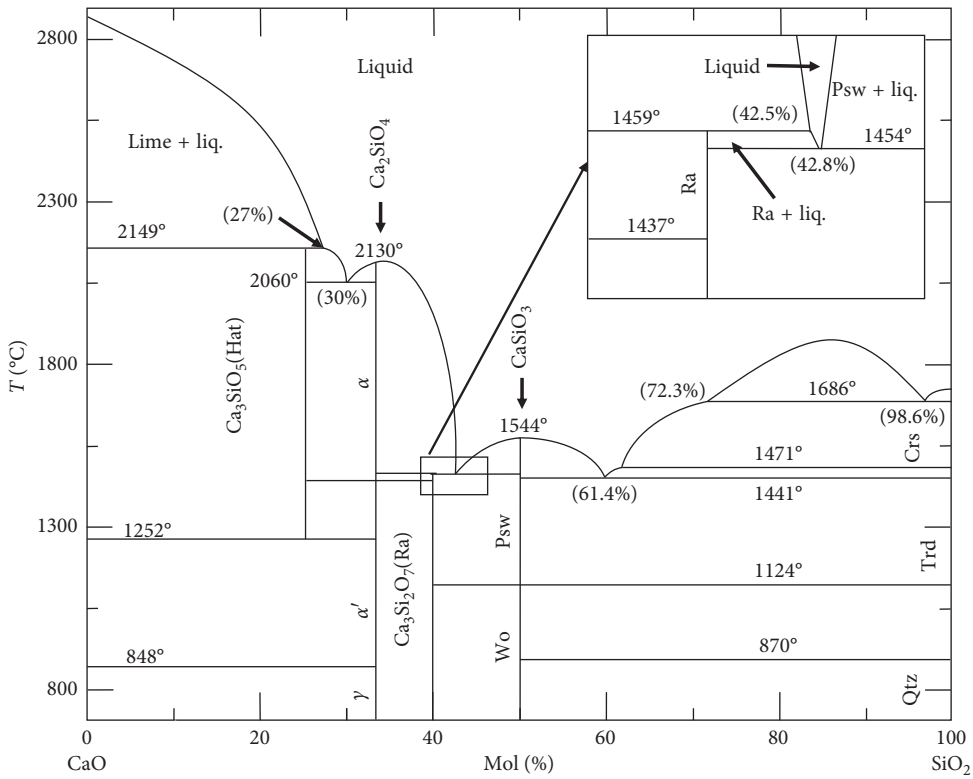

Figure 3: The CaO-SiO_2 phase diagram by Huang (1995) [28].

The measured temperatures are much lower than the corresponding calculated temperature. The main reason is that, in addition, the pyrometer used for measurement has area of measure approximately 2 mm in diameter, which means that it measures not only the combustion front temperature but also areas of preheating and cooling. In conclusion, the temperature measured corresponds to the average of the area of measurement.

The maximum combustion temperature was observed when an excess ($n = 3$) of fuel was used. The sharp increase in temperature indicates the ignition of the combustion reaction. The maximum temperature is referred to as combustion temperature, and after reaching the maximum temperature, the sample cools down rapidly. It can be observed that a dependence of the measured combustion temperature on the varying ratio, increasing the amount of fuel provides an increase in combustion temperature of the sample.

X-ray diffraction analysis of the combustion products obtained with different amounts of urea is shown in Figure 2. It can be observed that when $n = 1$, the powder showed poor crystallinity and the formed phases were α'-Ca_2SiO_4 (JCPDS file no. 00-036-0642), γ-Ca_2SiO_4 (JCPDS file no. 00-049-1672), CaO (JCPDS file no. 01-075-0264), and SiO_2 (JCPDS file no. 01-082-1564); probably, the starting materials used did not react as expected and therefore did not form a desired phase, thus causing the formation of the SiO_2 phase.

When the amount of urea was increased ($n = 2$), fully crystalline phase of wollastonite-2M was observed (JCPDS file no. 00-027-0088), indicating that the temperature achieved was sufficient to obtain the desired phase without subsequent calcination.

Further increase of amount urea ($n = 3$) provides the disappearance of wollastonite-2M phase and the appearance phases α'-Ca_2SiO_4 (JCPDS file no. 00-036-0642), γ-Ca_2SiO_4 (JCPDS file no. 00-049-1672), CaO (JCPDS file no. 01-075-0264), and SiO_2 (JCPDS file no. 01-082-1564). These phases have high crystallinity due to the high temperature of the synthesis, confirmed by the temperature measurements using the pyrometer (Figure 1). The higher combustion temperature provided by the large amount of fuel probably exceeded the melting temperature of wollastonite (as the calculated temperature predicts) and arrives directly to the liquid phase. As can be seen in the phase diagram (Figure 3), at a given temperature ($T = 1544^{\circ}C$), this phase has a congruent melting point. The direct passage to the liquid phase may have led to precipitation of the coexistent crystalline phases at the reached temperature during cooling.

Figure 4 shows infrared spectrum of all samples. The IR spectroscopic analysis data confirm that the IR peaks in the range of 480–1110 cm^{-1} are due to $CaSiO_3$ [9, 28]. The peaks in ~480 cm^{-1} can be attributed to the bending vibration Si–O–Si bond. Those bands within the range 900–1110 cm^{-1} were assigned to Si–O–Si asymmetric stretching vibration and the O–Si–O stretching vibration absorption band [29, 30]. The peak around 1370 cm^{-1} is attributed to the vibrations of ionic (NO_3), indicating the presence of trace amounts of nitrate from the starting material calcium nitrate in the sample; this peak decreases with the increase of the

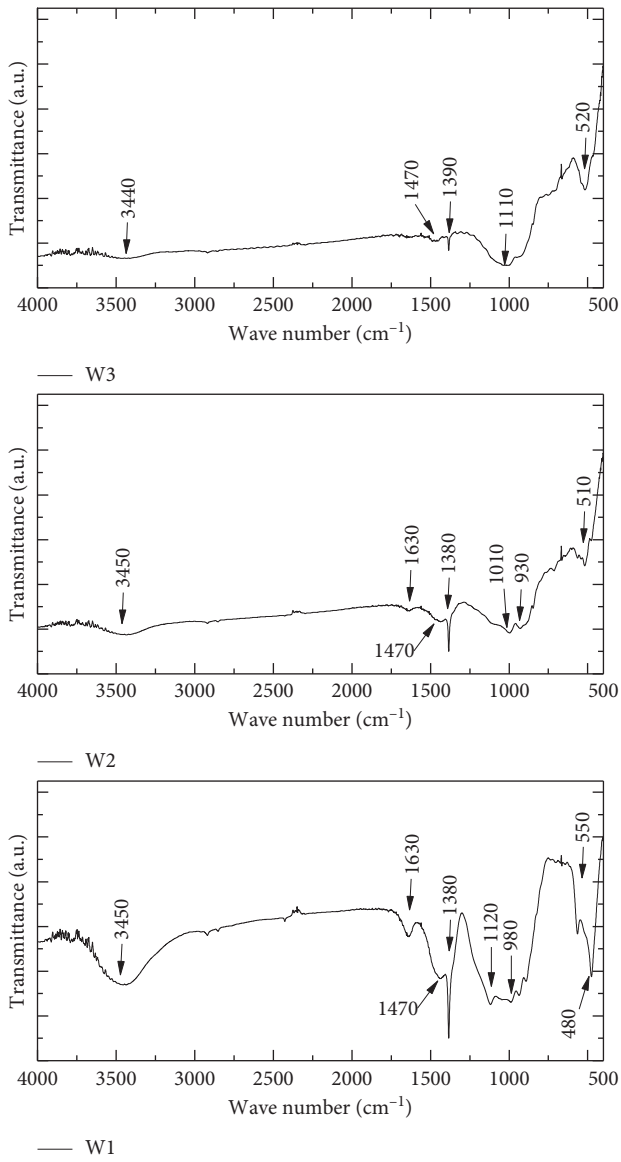

Figure 4: FTIR spectra of powders obtained from systems containing different amounts of urea.

Table 3: Influence of n ratio on the specific surface area and particle size of as-synthesized powders.

n ratio	SSA (m^2/g)	d_{BET} (nm)
1	15.7	130
2	7.2	280
3	15.6	130

amount of fuel [31]. The bands in the range 1470 cm^{-1}, when a sample was formed, show the presence of CaO in the sample, with the increase amount of fuel, and these bands progressively decreased [32, 33]. The band around 1644 cm^{-1} can be ascribed to be the bending vibration of the H–O–H bond in molecule water. A broad band around 3400–3600 cm^{-1} is caused by the stretching vibration of different kinds of hydroxyls and the remaining adsorbed water. With the increase in the amount of urea and consequently at the combustion temperature, these peaks disappear. The decrease could be attributed to the release of water molecules trapped inside the solid matrix [26, 34, 35].

Table 3 shows the specific surface area (SSA) and particle sizes (estimated from specific surface area (d_{BET}) of the powders obtained by combustion as a function of n. It is a well-established fact that, in combustion synthesis, the higher the combustion temperature, the longer the flame duration, leading to coarsening of the particles. Within the framework of this study, when $n = 1$, low flame temperature and high gas volume inhibited the particles growth and generated powder with higher surface area. As the amount of fuel increases, $n = 2$, the higher temperature during combustion reaction decreases the surface area due to grain growth. On the contrary, when $n = 3$, a possible melting and precipitation of new phases, caused by the high combustion temperature, provided a small particle size and high specific surface.

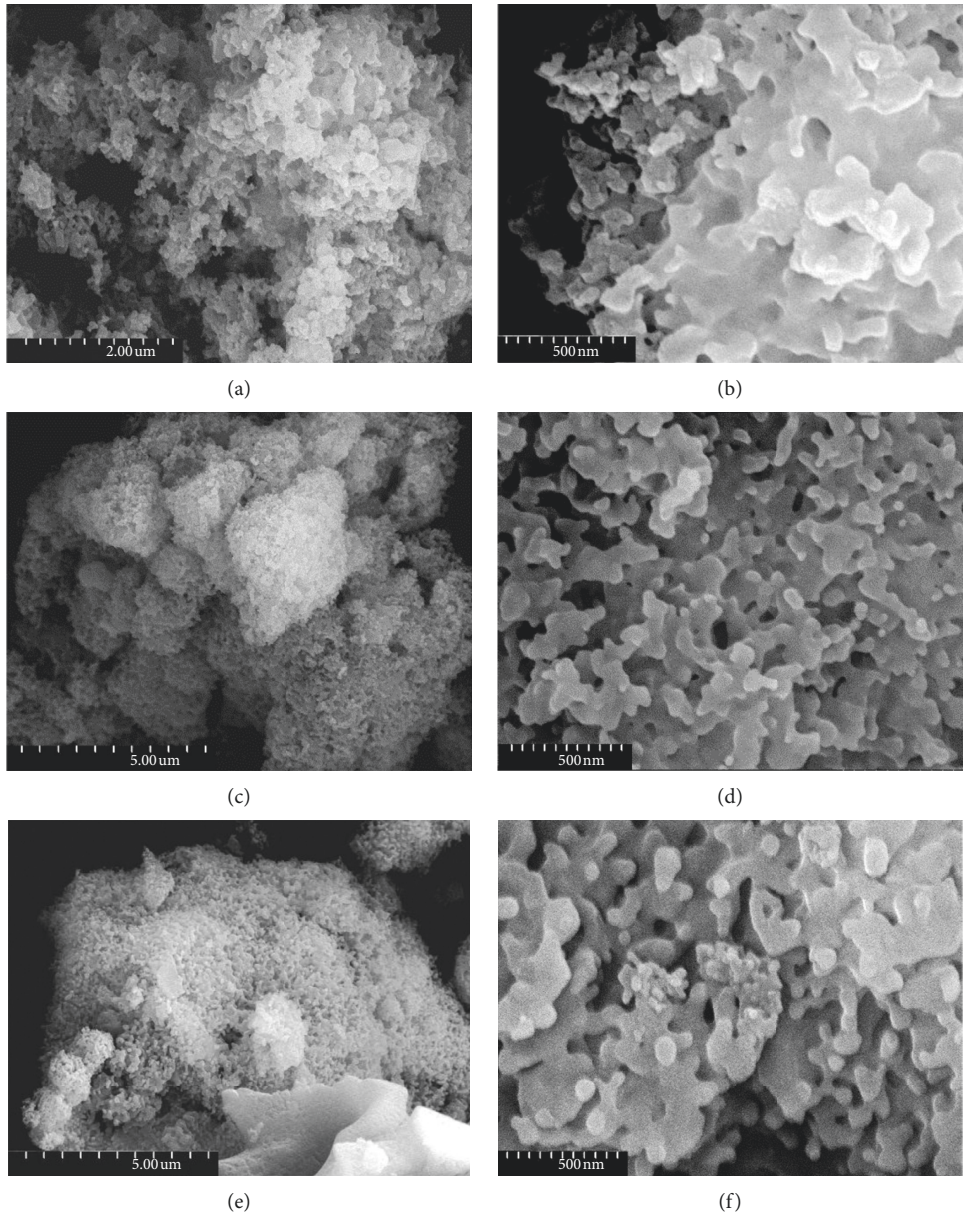

Figure 5: FESEM micrograph of the synthesized powders: (a, b) $n = 1$, (c, d) $n = 2$, and (e, f) $n = 3$.

FESEM observation of the product (Figure 4) shows that all samples exhibit particle nanostructures with nodular morphology which are quite agglomerated. At higher magnification (Figures 4(b), 4(d), and 4(f)), it is possible to observe that powders are structured submicronically and presented smaller particles were sintered together and form larger particles, which can be due to the high combustion temperature.

Figure 5(d) shows a greater presence of pores, when compared to samples shown in Figures 5(b) and 5(f), which is a microstructural characteristic of the products of combustion due to the escape of a large number of gases during the combustion; the increase of the amount of fuel (Figures 5(e) and 5(f)) provides a decrease in the presence of these pores, indicating a greater sintering of the particles.

In Figures 6(a) and 6(b), it is possible to observe another type of morphology of the samples obtained with $n = 1$ and $n = 3$, respectively, and a heterogeneous morphology is formed by a crystalline phase (clear part) surrounded by an amorphous phase (dark part). The heterogeneity can be confirmed from the analysis of the X-ray results (Figure 2) of these samples that evidence the formation of distinct phases. In the case of samples obtained with $n = 3$, where the phases found are crystalline, this can be explained due to the fact that the high combustion temperature was obtained that favoured the dissociation and decomposition of the wollastonite obtained when $n = 2$.

4. Conclusions

Crystalline $CaSiO_3$ has been synthesized by the solution combustion method without any thermal treatment after the synthesis.

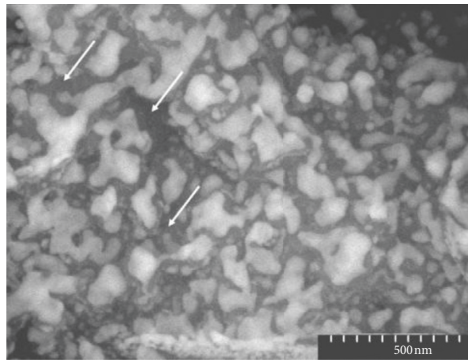

(a)

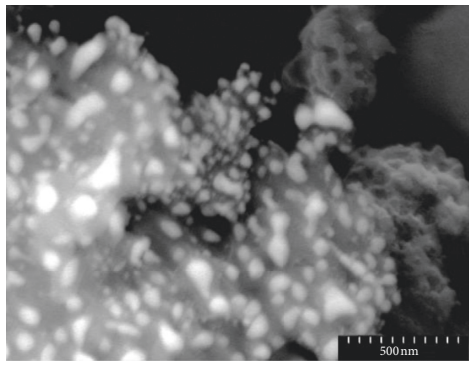

(b)

Figure 6: FESEM micrograph of the synthesized powders: (a) $n = 1$ and (b) $n = 3$.

It was observed that the amount of fuel significantly influences the composition of the phase.

When an excess of urea ($n = 2$) was used the wollastonite–2M was the only phase obtained.

The use of a stoichiometric amount of fuel ($n = 1$) did not favour the synthesis by combustion and consequently it was not possible to obtain crystalline phases of the material. While a higher amount of fuel ($n = 3$) provided the formation of calcium silicate phases, but it was not possible to obtain the wollastonite.

The combustion synthesis method for obtaining submicronic structured wollastonite, using urea as fuel, is an efficient method for obtaining powders without needing additional heat treatment.

Data Availability

The thermodynamic data used to support the findings of this study have been deposited in the *Lange's Handbook of Chemistry*, Dean, 1999 repository 10.1080/10426919008953291.

Conflicts of Interest

The authors declare that there are no conflicts of interest regarding the publication of this paper.

Acknowledgments

This work was funded by the Ministry of Economy and Competitiveness of Spain under Project MAT2013-48426-C2-1R and Program Science without Borders MEC/MCTI/CAPES/CNPq/FAPs (Call no. 03/2014), Process no. 401220/2014-1.

References

[1] Q. L. Loh and C. Choong, "Three-dimensional scaffolds for tissue engineering applications: role of porosity and pore size," *Tissue Engineering Part B: Reviews*, vol. 19, no. 6, pp. 485–502, 2013.

[2] N. K. Awad, S. L. Edwards, and Y. S. Morsi, "A review of TiO2 NTs on Ti metal: electrochemical synthesis, functionalization and potential use as bone implants," *Materials Science and Engineering: C*, vol. 76, pp. 1401–1412, 2017.

[3] S. Kunjalukkal Padmanabhan, F. Gervaso, M. Carrozzo, F. Scalera, A. Sannino, and A. Licciulli, "Wollastonite/hydroxyapatite scaffolds with improved mechanical, bioactive and biodegradable properties for bone tissue engineering," *Ceramics International*, vol. 39, no. 1, pp. 619–627, 2013.

[4] X. Liu and P. Ma, "Polymeric scaffolds for bone tissue engineering," *Annals of Biomedical Engineering*, vol. 32, no. 3, pp. 477–486, 2004.

[5] P. Khoshakhlagh, S. M. Rabiee, G. Kiaee et al., "Development and characterization of a bioglass/chitosan composite as an injectable bone substitute," *Carbohydrate Polymers*, vol. 157, pp. 1261–1271, 2017.

[6] B. Li, Z. Liu, J. Yang et al., "Preparation of bioactive β-tricalcium phosphate microspheres as bone graft substitute materials," *Materials Science and Engineering: C*, vol. 70, pp. 1200–1205, 2017.

[7] X. Wan, C. Chang, D. Mao, L. Jiang, and M. Li, "Preparation and in vitro bioactivities of calcium silicate nanophase materials," *Materials Science and Engineering: C*, vol. 25, no. 4, pp. 455–461, 2005.

[8] I. H. M. Aly, L. Abed Alrahim Mohammed, S. Al-Meer, K. Elsaid, and N. A. M. Barakat, "Preparation and characterization of wollastonite/titanium oxide nanofiber bioceramic composite as a future implant material," *Ceramics International*, vol. 42, no. 10, pp. 11525–11534, 2016.

[9] L. Fiocco, S. Li, M. M. Stevens, E. Bernardo, and J. R. Jones, "Biocompatibility and bioactivity of porous polymer-derived Ca-Mg silicate ceramics," *Acta Biomaterialia*, vol. 50, pp. 56–67, 2017.

[10] M. Magallanes-Perdomo, A. H. De Aza, I. Sobrados, J. Sanz, Z. B. Luklinska, and P. Pena, "Structural changes during crystallization of apatite and wollastonite in the eutectic glass of Ca_3 $(PO_4)_2$-$CaSiO_3$ system," *Journal of the American Ceramic Society*, vol. 100, no. 9, pp. 4288–4304, 2017.

[11] P. N. De Aza, Z. B. Luklinska, M. Anseau, F. Guitian, and S. De Aza, "Morphological studies of pseudowollastonite for biomedical application," *Journal of Microscopy*, vol. 182, no. 1, pp. 24–31, 1996.

[12] P. N. De Aza, F. Guitian, A. Merlos, E. Lora-Tamayo, and S. De Aza, "Bioceramics-simulated body fluid interfaces: PH and its influence of hydroxyapatite formation," *Journal of Materials Science: Materials in Medicine*, vol. 7, no. 7, pp. 399–402, 1996.

[13] P. N. De Aza, Z. B. Luklinska, M. R. Anseau, F. Guitian, and S. De Aza, "Bioactivity of pseudowollastonite in human saliva," *Journal of Dentistry*, vol. 27, no. 2, pp. 107–113, 1999.

[14] P. N. De Aza and Z. B. Luklinska, "Effect of glass-ceramic microstructure on its in vitro bioactivity," *Journal of Materials Science: Materials in Medicine*, vol. 14, no. 10, pp. 891–898, 2003.

[15] P. N. de Aza, F. Guitian, and S. de Aza, "Bioactivity of wollastonite ceramics: in vitro evaluation," *Scripta Metallurgica et Materialia*, vol. 31, no. 8, pp. 1001–1005, 1994.

[16] P. N. De Aza, F. Guitian, and S. De Aza, "Polycrystalline wollastonite ceramics. Biomaterials free of P_2O_5," in *Advances in Science and Technology: Materials in Clinical Applications*, P. Vicenzini, Ed., pp. 19–27, 1995.

[17] C. Wu, J. Chang, W. Zhai, and S. Ni, "A novel bioactive porous bredigite ($Ca_7MgSi_4O_{16}$) scaffold with biomimetic apatite layer for bone tissue engineering," *Journal of Materials Science: Materials in Medicine*, vol. 18, no. 5, pp. 857–864, 2007.

[18] R. Abd Rashid, R. Shamsudin, M. A. Abdul Hamid, and A. Jalar, "Low temperature production of wollastonite from limestone and silica sand through solid-state reaction," *Journal of Asian Ceramic Societies*, vol. 2, no. 1, pp. 77–81, 2014.

[19] A. Udduttula, S. Koppala, and S. Swamiappan, "Sol-gel combustion synthesis of nanocrystalline wollastonite by using glycine as a fuel and its in vitro bioactivity studies," *Transactions of the Indian Ceramic Society*, vol. 72, no. 4, pp. 257–260, 2013.

[20] R. Morsy, R. Abuelkhair, and T. Elnimr, "Synthesis and in vitro bioactivity mechanism of synthetic α-wollastonite and β-wollastonite bioceramics," *Journal of Ceramic Science and Technology*, vol. 7, no. 1, pp. 65–70, 2016.

[21] M. A. Aghayan and M. A. Rodríguez, "Influence of fuels and combustion aids on solution combustion synthesis of bi-phasic calcium phosphates (BCP)," *Materials Science and Engineering: C*, vol. 32, no. 8, pp. 2464–2468, 2012.

[22] X.-H. Huang and J. Chang, "Synthesis of nanocrystalline wollastonite powders by citrate–nitrate gel combustion method," *Materials Chemistry and Physics*, vol. 115, no. 1, pp. 1–4, 2009.

[23] S. L. González-Cortés and F. E. Imbert, "Fundamentals, properties and applications of solid catalysts prepared by solution combustion synthesis (SCS)," *Applied Catalysis A: General*, vol. 452, pp. 117–131, 2013.

[24] A. S. Mukasyan, P. Epstein, and P. Dinka, "Solution combustion synthesis of nanomaterials," *Proceedings of the Combustion Institute*, vol. 31, no. 2, pp. 1789–1795, 2007.

[25] K. C. Patil, S. T. Aruna, and T. Mimani, "Combustion synthesis: an update," *Current Opinion in Solid State and Materials Science*, vol. 6, no. 6, pp. 507–512, 2002.

[26] R. P. Sreekanth Chakradhar, B. M. Nagabhushana, G. T. Chandrappa, K. P. Ramesh, and J. L. Rao, "Solution combustion derived nanocrystalline macroporous wollastonite ceramics," *Materials Chemistry and Physics*, vol. 95, no. 1, pp. 169–175, 2006.

[27] J. A. Dean, *Lange's Handbook of Chemistry*, 15th ed., 1999.

[28] S. Atalay, H. I. Adiguzel, and F. Atalay, "Infrared absorption study of Fe_2O_3-CaO-SiO_2 glass ceramics," *Materials Science and Engineering: A*, vol. 304–306, no. 1–2, pp. 796–799, 2001.

[29] X. Chen, J. Jiang, F. Yan, S. Tian, and K. Li, "A novel low temperature vapor phase hydrolysis method for the production of nano-structured silica materials using silicon tetrachloride," *RSC Advances*, vol. 4, no. 17, p. 8703, 2014.

[30] R. K. Nariyal, P. Kothari, and B. Bisht, "FTIR Measurements of SiO_2 Glass Prepared by Sol-Gel Technique," *Chemical Science Transactions*, vol. 3, no. 3, pp. 1064–1066, 2014.

[31] P. Saravanapavan and L. L. Hench, "Mesoporous calcium silicate glasses. I. Synthesis," *Journal of Non-Crystalline Solids*, vol. 318, no. 1–2, pp. 1–13, 2003.

[32] K. A. Almasri, H. A. A. Sidek, K. A. Matori, and M. H. M. Zaid, "Effect of sintering temperature on physical, structural and optical properties of wollastonite based glass-ceramic derived from waste soda lime silica glasses," *Results in Physics*, vol. 7, pp. 2242–2247, 2017.

[33] R. Lakshmi, V. Velmurugan, and S. Sasikumar, "Preparation and phase evolution of Wollastonite by sol-gel combustion method using sucrose as the fuel," *Combustion Science and Technology*, vol. 185, no. 12, pp. 1777–1785, 2013.

[34] C. Wang, D. Wang, and S. Zheng, "Characterization, organic modification of wollastonite coated with nano-$Mg(OH)_2$and its application in filling PA_6," *Materials Research Bulletin*, vol. 50, pp. 273–278, 2014.

[35] N. Tangboriboon, T. Khongnakhon, S. Kittikul, R. Kunanuruksapong, and A. Sirivat, "An innovative $CaSiO_3$ dielectric material from eggshells by sol–gel process," *Journal of Sol-Gel Science and Technology*, vol. 58, no. 1, pp. 33–41, 2011.